Available online at www.sciencedirect.com

ScienceDirect

Procedia CIRP 14 (2014) 281 – 286

www.elsevier.com/locate/procedia

6th CIRP International Conference on High Performance Cutting, HPC2014

Finite Element Simulation and Experimental Validation of Residual Stresses in High Speed Dry Milling of Biodegradable Mg-Ca Alloys

M. Salahshoor, Y.B. Guo*

Dept. of Mechanical Engineering, The University of Alabama, Tuscaloosa, AL 35487, USA

* Corresponding author. Tel.: +1 205 348 2615; Fax: +1 205 348 6419. *E-mail address:* yguo@eng.ua.edu

Abstract

Magnesium-Calcium (Mg-Ca) alloys have become attractive biodegradable orthopedic biomaterials recently. Residual stresses are proven to be very influential on the degradation rate of an Mg-Ca implant in the human body. Due to the time and cost reasons, development of finite element models to predict residual stress profiles in cutting of Mg-Ca implants is highly desirable. In this study, a finite element simulation model of orthogonal cutting without explicit chip formation has been developed by using the plowing depth approach in order to predict process-induced residual stresses in high speed dry cutting of Mg-Ca0.8 (wt %) alloy using diamond tools. Mechanical properties of Mg-Ca0.8 biomaterial at high strain rates and large strains were determined using the split-Hopkinson pressure bar test. The internal state variable (ISV) plasticity model has been implemented to model the dynamic material behavior under cutting regimes. The residual stress evolution and effects of plowing speed and plowing depth on residual stress profiles are studied. Residual stress measurements were also performed utilizing the X-ray diffraction technique for validation purposes.

Selection and peer-review under responsibility of the International Scientific Committee of the 6th CIRP International Conference on High Performance Cutting

Keywords: Residua stess; dry cutting; magnesium alloy; implants

1. Introduction

The in-service performance of machined components substantially depends on surface integrity, particularly residual stresses at or near the machined surface [1,2]. Residual stresses directly influence deformation, static and dynamic strength, chemical resistance, electromagnetic, optical, acoustical, and thermal properties of mechanical and electrical components [3]. They are generated by individual or combined effects of mechanical, thermal, and metallurgical impacts in machining processes. Machining process parameters determine the intensity of the mentioned impacts and ultimately the magnitude, penetration depth, profile shape, and type of the induced residual stresses. Therefore, understanding the correlation between process parameters and induced residual stresses is a fundamental step towards realizing the manufacturing for performance concept. However, measuring a residual stress profile using popular XRD is very time consuming. In an effort to study process parameter-residual stress correlations more economically and efficiently, researchers have sought to develop predictive models to calculate induced residual stress profiles in machining processes since three decades ago.

Many researchers have developed simulation models to predict residual stress. Sasahara et al [4] and Liu and Guo [5] found that tensile residual stress layer made by one pass roughing could turned into a compressive one by subsequent fine cutting pass. Liu and Guo [5] also showed that residual stress predictions were sensitive to friction at tool-chip interface.

Jacobus et al [6] developed a plane strain thermoelastoplastic model of metal flow under the flank of the cutting tool to predict in-plane biaxial residual stress profiles. Later, Jacobus et al [7] extended this model to accommodate for the more complex process geometry associated with turning. Both prediction and experiment showed that increase in feed and depth of cut lead to increase in workpiece

Selection and peer-review under responsibility of the International Scientific Committee of the 6th CIRP International Conference on High Performance Cutting
doi:10.1016/j.procir.2014.03.062

temperatures and, subsequently, to increase in the tensile character of the residual stresses at and near the surface.

A few studies [8-10] simulated the influence of the cutting edge geometry on residual stresses. Very fine mesh around the cutting edge and machined surface is required to provide adequate spatial resolution [11-13]. Larger and more refined models translate into more digital storage, computational time, and expensive simulations. Guo et al [14] proposed a new modeling approach without chip formation based on the concept of plowed depth. This approach avoids the severe element distortion and provides enough spatial resolution to capture sharp deformation gradients. Meanwhile, it still reflects the realistic stagnation phenomenon in cutting.

Previous studies have shown that residual stress state after cutting is strongly influenced by material properties [10]. Magnesium-calcium (Mg-Ca) alloys have emerged as very appealing biomaterials to avoid stress shielding for orthopedic applications [15,16]. However, these alloys degrade quickly in body environment and there is a dire need for alternatives to control their degradation rate. Denkena and Lucas [17] were able to decrease this rate by adjusting surface integrity particularly residual stresses.

The objective of this study is to predict process-induced residual stress profiles in cutting novel Mg-Ca0.8 biomaterial using FEA method. To meet this objective: (i) an FE model without explicit chip formation is developed; (ii) an internal state variable plasticity model is implemented to enhance the capability for predicting mechanical behavior of the material under prevalent cutting regimes; (iii) residual stress measurements are performed for validation purposes. Moreover, noticing the difficulty of some parametric evaluations experimentally, the effects of plowing speed and plowing depth on residual stress profiles are studied using the developed FE model.

2. Material Model

Workpiece material usually experiences large strains, high strain rates, high temperatures, Bauschinger effect, and complex loading histories throughout a cutting operation at various length scales. A dislocation based internal state variable (ISV) plasticity model developed by Bammann et al [18] is used to describe the complex thermomechanical deformation state of the material. The constitutive model is formulated with respect to stress free configuration and can be written as follow for uniaxial tension and compression:

$$\sigma = \alpha + \kappa + Y(\theta) + V(\theta) sinh^{-1}(|\dot{\varepsilon}|/f(\theta)) \quad (1)$$

$$\alpha = \sqrt{h\dot{\varepsilon}/(r_d\dot{\varepsilon} + r_s)}\tanh(\sqrt{h(r_d\dot{\varepsilon} + r_s)/\dot{\varepsilon}}\ \varepsilon) \quad (2)$$

$$\kappa = \sqrt{H\dot{\varepsilon}/(R_d\dot{\varepsilon} + R_s)}\tanh(\sqrt{H\dot{\varepsilon}(R_d\ \dot{\varepsilon} + R_s)/\dot{\varepsilon}}\ \varepsilon) \quad (3)$$

The evolution equations (2) and (3) of internal state variables α and κ are motivated from dislocation mechanics and are in hardening minus recovery format. Dynamic recovery due to dislocation cross slip and thermal recovery due to diffusion controlled vacancy assisted climb of dislocations are taken into account in deriving the evolution equations. α represents kinematic hardening and captures the softening effect, termed as Bauschinger effect, due to unloading. κ represents isotropic hardening and captures the continued hardening at large strains. The use of internal state variables and the evolution equations enable the prediction of strain rate history and temperature history effects as well.

The model uses nine temperature *(θ)* dependent functions to describe the plastic response [19]. They can be classified into three groups: initial yield, recovery, and hardening functions. The rate-independent yield stress *Y(θ)*, the rate-dependence of initial yield stress *f(θ)*, and the magnitude of rate-dependence of yield stress *V(θ)* are assumed to be of the following forms:

$$V(\theta) = C_1 \exp(-C_2/\theta) \quad (4)$$

$$Y(\theta) = C_3 \exp(C_4/\theta)([1 + (\tanh(C_{19}(C_{20} - \theta))]/2) \quad (5)$$

$$f(\theta) = C_5 \exp(-C_6/\theta) \quad (6)$$

The three functions of $r_d(\theta)$, $h(\theta)$, and $r_s(\theta)$ describe the kinematic hardening and recovery, which can be thought of as the center of yield surface. The functions of $R_d(\theta)$, $H(\theta)$, and $R_s(\theta)$ describe the isotropic hardening and recovery, which can be thought of as the radius of the yield surface:

$$r_d(\theta) = C_7 \exp(-C_8/\theta) \quad (7)$$

$$h(\theta) = C_9 - C_{10}\theta \quad (8)$$

$$r_s(\theta) = C_{11} \exp(-C_{12}/\theta) \quad (9)$$

$$R_d(\theta) = C_{13} \exp(-C_{14}/\theta) \quad (10)$$

$$H(\theta) = C_{15} - C_{16}\theta \quad (11)$$

$$R_s(\theta) = C_{17}\exp(-C_{18}/\theta) \quad (12)$$

The material constants (C_1-C_{20}) in equations (4~12) are determined by fitting the ISV model to stress-strain data obtained from quasi-static and dynamic compression tests. The extracted constants for Mg-Ca0.8 biomaterial, material shear and bulk moduli *K* and *G*, melting temperature, initial temperature, heat coefficient, and damage parameters were incorporated into Abaqus via a user modified material subroutine VUMAT [20].

3. Residual Stress Prediction Model

Guo et al [21] investigated chip morphology transition under the influence of cutting edge geometry and introduced a novel hybrid modeling approach [14] without explicit chip formation to predict cutting-induced residual stresses. This modeling approach is built upon the concept of plowed depth and material stagnation ahead of the cutting edge. As is shown in schematic Fig. 1, material flows towards the cutting edge until it reaches to the material stagnation zone in the vicinity of point P. The presence of stagnation zone in cutting has been

shown both experimentally in conventional cutting [22] and numerically in precision cutting [11,21] and nanocutting [23]. Material flow splits into upward and downward streams at stagnation zone. Upward stream forms chip and downward stream forms the machined surface. The formed chip leaves the rake face of the cutting tool at point A and at point B, tool loses contact with machined surface. Plowed depth δ is a fraction of uncut chip thickness d located between ideal material separation line BD and actual separation line PC. This depth of material becomes squashed by the cutting edge and experiences high transient stresses, large strains and strain rates at high temperatures with severe gradients. It is legitimately hypothesized that the plowed layer is the key element contributing to residual stress generation in near surface zone of machined surfaces. Therefore, the chip forming stream of material flow above the actual separation line PC is neglected in the proposed numerical modeling approach.

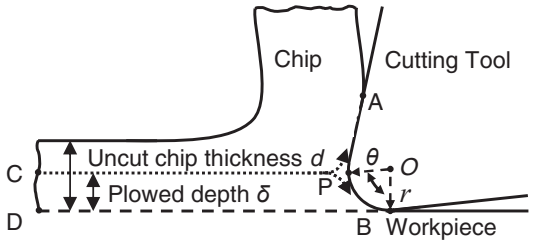

Fig. 1 Schematic of ploughed depth and material stagnation in a cutting process [14].

The plowed depth δ depends on cutting edge geometry and workpiece material. It is calculated using $\delta = r \times (1 - \cos\theta)$ where r is cutting edge radius and θ is stagnation angle. A wide range of published work has shown that the stagnation angle varies from 20° to 50° for most cutting edge geometry and work materials [22]. The stagnation angles used in this study are 20°, 26°, and 32° corresponding respectively to 0.6, 1.0, and 1.5 µm plowed depth. Higher stagnation angles caused severe element distortion and ultimately simulations failed despite the fact that adaptive mesh was used in near surface layers of the model. This may indicate that the upper limit of stagnation angle is about 32° for this combination of Mg-Ca0.8 (wt%) alloy and tool geometry. However, the later statement needs to be verified experimentally.

The converged mesh shown in Fig. 2 represents the 2-dimensional orthogonal cutting of Mg-Ca0.8 (wt%) alloy. The cutting edge radius r is 10 µm representing a sharp cutting edge. Rake angle α and clearance angle λ are 12° and 6°, respectively. Cutting temperature of the tool/workpiece system is determinative of generated residual stresses. On the other hand, realistic computation of cutting temperature involves considering thermal interactions of tool/workpiece system with environment through convection, radiation, and conduction. In this context, both tool and workpiece are meshed using plane strain elements with temperature degree of freedom. The tool is constrained to move horizontally at a constant speed after initial vertical penetration into the workpiece surface till it reaches the plowed depth amount. The overall dimensions of the workpiece are set to be 500 µm × 200 µm to avoid both size and edge effects and also to provide efficient computation time. The bottom layer of the workpiece is modeled with semi-infinite elements to prevent stress bounce back. Workpiece mesh becomes finer moving towards the surface and elements in the first 10 layers are as small as 1 µm. The initial temperature of tool and workpiece is 20 °C.

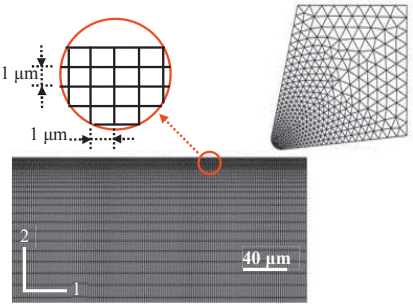

Fig. 2 FE mesh of residual stress prediction using ploughed depth concept.

Inelastic deformation and friction at tool/workpiece interface generate heat during cutting process. The dominant heat transfer mode, especially in dry cutting, is conduction and the total dissipated heat due to convection and radiation is about 20% [24]. The tool/workpiece interface is assumed to be perfectly conductive due to intimate contact between adjacent surfaces under high cutting pressures. However, tool and workpiece will receive different shares of the generated heat depending on their thermal properties (Table 1). Heat flux partition of tool and workpiece are calculated using following equations [24]:

$$R_W = 1/(1 + 1.5 \times (\lambda_T/\lambda_W) \times \sqrt{\alpha_W/\alpha_T}) \quad (13)$$

$$R_T = 1 - R_W \quad (14)$$

$$\alpha = \lambda/(c_p \times \rho) \quad (15)$$

Table 1. Thermal properties of PCD tool and Mg-Ca0.8 alloy

Material	C_p[J/Kg.K]	λ[W/m.K]	α [m^2/s]	β [µm/m.K]
PCD [29]	509	2000	1.12×10^{-3}	1.18
Mg-Ca0.8	1010	72	4.07×10^{-5}	26

Substituting appropriate values from Table 1 into equations 13 to 15 result in R_w = 11% and R_T = 89% meaning 89% of the generated heat diffuses into PCD tool and only 11% stays in the workpiece. Guo et al [14] modified the VUMAT subroutine to include frictional heat in addition to inelastic deformation heat as well as heat transfer between workpiece and surrounding environment in numerical analysis of cutting. This subroutine, used in this study, implements ISV plasticity model of the workpiece mechanical behavior and elastic properties of the PCD tool (Table 2).

A total of seven simulation cases (Table 3) were performed to study the effect of plowed depth and cutting speed on induced residual stresses. Each simulation case consists of

two-step analysis. At first step, tool plows the workpiece surface which is accomplished in ABAQUS/Explicit. Transient mechanical state of the workpiece including stresses, strains, and temperatures is computed in a dynamic coupled temperature-displacement analysis. At step two, computed transient mechanical state is imported into ABAQUS/Standard and the workpiece is cooled down to room temperature. As such, transient stresses relax till residual stresses develop at room temperature.

Table 2. Elastic properties of PCD tool and Mg-Ca0.8 alloy

Material	ρ [Kg/m^3]	E [GPa]	ν
PCD [25]	3500	1220	0.20
Mg-Ca0.8	1750	45	0.33

Table 3. Cutting speed and plowed depth in residual stress prediction cases

Cutting speed V [m/min]	Plowed depth δ [μm]
1200	0.6, 1.0, 1.5
1600	0.6
2000	0.6
2400	0.6
2800	0.6

4. Cutting Setup and Residual Stress Measurements

Disc-shaped samples made of lab-made Mg-Ca0.8 alloy were face milled in a 3 axis Cincinnati Arrow 500 CNC machine. No coolant was applied throughout the tests. Nine diamond tipped milling inserts were clamped in a 127 mm diameter face mill. Resulting angles at the cutting edge were axial rake 12° and axial relief 6°. The cutting speed was in 1200-2800 m/min range while the depth of cut and feed were held constant at 200 μm and 200μm/rev, respectively. A detailed description of the experimental setup is given in [20]. Cutting-induced residual stresses on the machined surfaces were measured using 4-axis Bruker D8 XRD machine and $\sin^2\psi$ method. X-rays with λ = 0.1542 nm wavelength were generated applying 35 mA and 40 kV power to X-ray tube with cupper target. X-rays were collimated and directed onto the sample's surface using 0.8 mm diameter collimator. An area detector located 15 cm far from the goniometer's center collected diffracted X-rays. {1 2 -3 3} crystallographic planes corresponding to 2θ = 118.48° angle were used to measure residual strains. The stress state was assumed to be plane stress (σ_3 = 0) and uniform within the diffracting volume. Modulus of elasticity (E = 45 GPa) and Possion's ratio (υ = 0.33) of the polycrystalline Mg-Ca0.8 were used in computing residual stresses and they were assumed to be isotropic within the diffracting volume. Electropolishing technique was implemented to remove the material layer by layer in order to measure subsurface residual stresses.

5. Results and Discussions

5.1. Residual stress evolution

Fig. 3 shows how stresses along a straight, in-depth path evolve to eventually become residual stresses at and near the machined surface. Transient profile refers to stress distribution right below the cutting edge while cutting process is under progress. There is a sharp stress gradient in the first 12 μm below the surface during the cutting. Due to fast cutting speeds, generated heat does not have enough time to diffuse away. As such, considerable thermal strains are superimposed on mechanical strains to stretch the surface layers. However, layers below the HAZ zone constrain the stretching and cause large compressive stresses at or near the surface while the cutting is in progress.

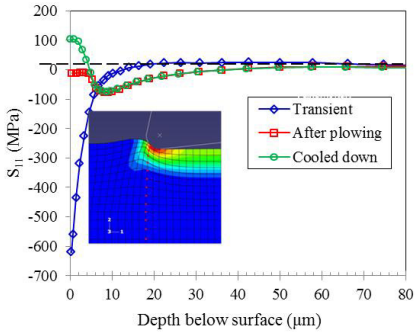

Fig. 3 Residual stress evolution in machined Mg-Ca0.8 surface (V = 1200 m/min; δ = 0.6 μm).

When the cutting/plowing is over, significant portion of the thermal strains is relaxed since the generated heat has had more time to spread around in the surrounding media. Therefore, surface layers tend to shrink. On the other hand, according to Hertzian contact theory maximum contact pressure and mechanical deformation has happened below the surface. This means that subsurface material layers are mechanically stretched due to compressing action of the thrust force. At the end of the cutting process, the tendency of the HAZ layer to shrink faces with some constraint by the plastically stretched subsurface layers. This causes more tensile stresses at closer to surface layers and more compressive stresses at deeper layers in the material. Giving the machined surface more time in order to cool down to room temperature leads to more shrinkage tendency in HAZ layer. This causes even more tensile residual stresses at the surface and in about 5 μm below the surface. At this point, residual stress profile has established its characteristic hook shape as is shown in Fig. 3.

5.2. Cutting speed effect on residual stress profile

Fig. 4 shows residual stress profiles at machined surface layer developed under different cutting speeds. To analyze our observation in Fig. 4, it would be helpful if we go back and pay attention to the process by which the machined surface is

formed in Fig. 1. Each material element located in plowed-depth layer experiences an extrusion like deformation as it approaches to cutting edge and becomes part of the machined surface past point B. This deformation field would govern the machined surface formation process regardless of the rate by which the deformation takes place. However, material elements would require more energy to experience same amount of deformation under higher rate than they would under lower rate. That translates into more heat generation under higher cutting speeds, considering the fact that majority of the inelastic deformation energy dissipates into heat. Therefore, cutting speed effect on residual stress profile is expected to be more of a thermal rather than mechanical nature. In this context, it is anticipated to observe more tensile residual stresses at machined layer under higher cutting speeds. However, the predicted results in Fig. 4 does not support this expectation and cutting speed shows almost effect less on residual stress profiles in cutting Mg-Ca0.8 using diamond tool. The missing piece should be something that suppresses thermal effect of the cutting speed. A possible way is taking out the generated heat from the deformation field fast enough to avoid thermal softening and subsequent excessive stretching in subsurface layers. Revisiting Table 1 reveals that this potential possibility could be an occurring reality. Diamond has super heat conduction property and acts as a heat sink which suppresses thermal effect of cutting speed on residual stress profiles.

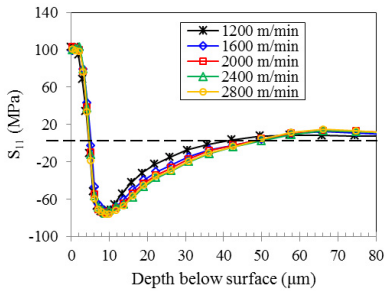

Fig. 4 Effect of cutting speed on residual stress profiles of machined Mg-Ca0.8 (δ = 0.6 μm).

5.3. Plowing depth effect on residual stress profile

Fig. 5 shows the effect of plowing depth on residual stress profiles in the machined surface layer of the Mg-Ca0.8 workpiece. Increasing plowed depth from δ = 0.6 μm to δ = 1.5 μm (almost three times increase) shows marginal influence on the tensile portion of the residual stress profiles as opposed to more noticeable influence on compressive portion of the profiles. This speaks on the fact that plowing depth has more of a mechanical rather than thermal effect on residual stress profiles. It is predicted that deeper plowing will shift the location of the maximum compressive stress to deeper subsurface layers and will increase the total thickness of the compressively stressed layers (~ 70 μm for δ = 1.5 μm). However, magnitude of the maximum subsurface residual stress decreases with increasing the plowing depth.

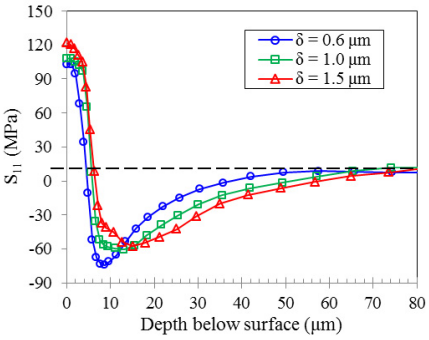

Fig. 5 Effect of plowing depth on residual stress profiles of machined Mg-Ca0.8 (V = 1200 m/min).

6. Experimental Validation and Discussion

Fig. 6 shows a representative case where measured residual stress profile at and near the machined surface is compared with the predicted profile. There is a noticeable difference between measurement and prediction at the surface. This might be partially due to the presence of feed marks and preexisting residual stresses on the actual machined surface which are neglected in the numerical model. Meanwhile, taking into account the inherent uncertainty of the X-ray diffraction method and the exact value of the actual plowing depth, there is a reasonable agreement among prediction and measurements at subsurface layers. Uncertainty in the measurement and plowing depth and neglecting surface roughness and preexisting residual stresses in the model are among the contributing error sources for observed discrepancies in Fig. 6. Another source of error would be the deformation patterns by which each of the measured and predicted residual stresses are created. While predictions are extracted from an orthogonal cutting model, measured values are caused by a three-dimensional face milling operation. Although details like cutting geometry, effective cutting parameters, corner radius, and cutting sequence set the three-dimensional cutting considerably apart from the orthogonal cutting, both operations follow same fundamental mechanics in generating the finished surface [8]. “The finished surface is

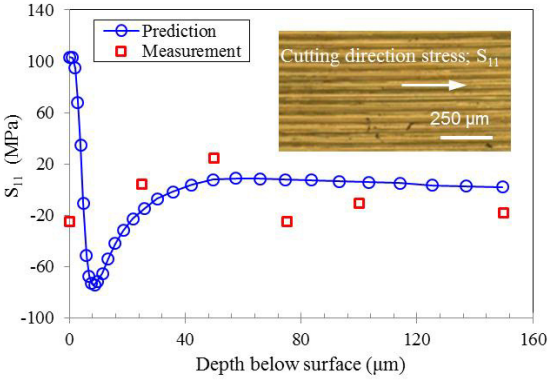

Fig. 6 Residual stress predictions and measurements (V = 1200 m/min; δ = 0.6 μm).

generated through elastic-plastic deformation in front of the cutting tool as the tool edge separates chips from the machining surface". In this context, orthogonal modeling could be used as a first approximation for three-dimensional operation to analyze the effects of process parameters on residual stress profiles particularly in the subsurface as is shown in Fig. 6. It is also noticed that there is a sharp gradient of residual stress in the first 20 μm below the machined surface by prediction which would be either overlooked in measurements for efficiency and economical reasons or considerably erroneous, if not impossible, to measure due to the size effect of the interacting volume of the material with the X-rays (5 ~ 20 μm deep [3]). Therefore, the possibility of having very fine spatial resolution would and should remain as a key characteristic of numerical techniques to make them viable in competing with measurement techniques.

7. Conclusions

A finite element model without explicit chip formation is developed to predict process-induced residual stress profiles in orthogonal cutting of the novel Mg-Ca0.8 biomaterial. Complex thermomechanical behavior of the material is captured applying an internal state variable plasticity model. The key findings of this study are as follow:

- Residual stresses evolve from a transient, highly compressive, and L-shaped profile to a stable, hook-shaped profile which starts with tensile stresses at the surface and reaches to more moderate compressive residual stresses at deeper subsurface layers.
- Super hear conduction property of the diamond tool suppresses the thermal effect of the cutting speed and avoids the change in residual stress profiles with respect to the cutting speed.
- Deeper plowing shifts the maximum compressive stress location to deeper subsurface layers and increases the thickness of the subsurface layer which is covered by compressive residual stresses.
- The predictions are good first approximation of the measured residual stresses particularly at subsurface layers.

Acknowledgements

The work was supported by NSF CMMI #1000706.

References

[1] F. Hashimoto, Y.B. Guo, A.W. Warren, 2006, "Surface integrity difference between hard turned and ground surfaces and its impact on fatigue life," Ann. of the CIRP 55/1 (2006) 81-84.
[2] I.S. Jawahir, E. Brinksmeier, R. M'Saoubi, D.K. Aspinwall, J.C. Outeiro, D. Meyer, D. Umbrello, A.D. Jayal, Surface integrity in material removal processes: recent advances, CIRP Ann. – Manuf. Tech. 60 (2011) 603-626.
[3] E. Brinksmeier, J.T. Cammett, W. König, P. Leskovar, J. Peters, H.K. Tönshoff, Residual stresses-measurement and causes in machining processes, Ann. of the CIRP 31 (1982) 491-510.
[4] H. Sasahara, T. Obikawa, T. Shirakashi, FEM analysis of cutting sequence effect on mechanical characteristics in machined layer, J. Mater. Process. Tech. 62 (1996) 448-453.
[5] C.R. Liu, Y.B. Guo, Finite element analysis of the effect of sequential cuts and tool-chip friction on residual stresses in a machined layer, Int. J. Mech. Sci. 42 (2000) 1069-1086.
[6] K. Jacobus, R.E. DeVor, S.G. Kapoor, Machining-induced residual stress: experimentation and modeling, J. Manuf. Sci. E. – T. ASME 122 (2000) 20-31.
[7] K. Jacobus, R.E. DeVor, S.G. Kapoor, R.A. Peascoe, Predictive model for the full biaxial surface and subsurface residual stress profiles from turning, J. Manuf. Sci. E. – T. ASME 123 (2001) 537-546.
[8] H. Sasahara, T. Obikawa, T. Shirakashi, Prediction model of surface residual stress within a machined surface by combining two orthogonal plane models, Int. J. Mach. Tool. Manuf. 44 (2004) 815-822.
[9] W.J. Zong, D. Li, K. Cheng, T. Sun, Y.C. Liang, Finite element optimization of diamond tool geometry and cutting-process parameters based on surface residual stresses, Int. J. Adv. Manuf. Tech. 32 (2007) 666-674.
[10] V. Schulze, H. Autenrieth, M. Deuchert, H. weule, Investigation of surface near residual stress states after micro-cutting by finite element simulation, CIRP Ann. – Manuf. Techn. 59 (2010) 117-120.
[11] K.C. Ee, O.W. Dillon Jr., I.S. Jawahir, Finite element modeling of residual stresses in machining induced by cutting using a tool with finite edge radius, Int. J. Mech. Sci. 47 (2005) 1611-1628.
[12] J.C. Outeiro, D. Umbrello, R. M'Saoubi, Experimental and numerical modeling of the residual stresses induced in orthogonal cutting of AISI 316L steel, Int. J. Machine Tools Manuf. 46 (2006) 1786-1794.
[13] T. Özel, E. Zeren, Finite element modeling the influence of edge roundness on the stress and temperature fields induced by high-speed machining, Int. J. Adv. Manuf. Technol. 35 (2007) 255-267.
[14] Y.B. Guo, S. Anurag, I.S. Jawahir, A novel hybrid predictive model and validation of unique hook-shaped residual stress profile in hard turning, CIRP Ann. – Manuf. Techn. 58 (2009) 81-84.
[15] F.W. Bach, B. Denkena, K. Weinert, P. Alpers, M. Bosse, N. Hammer, Influence of cutting and non-cutting processes on the corrosion behavior and the mechanical properties of magnesium alloys, Proc. 7th Int. Conf. Magnesium Alloys and Their Applications (2007) 1076-1084.
[16] N. Von der Hoh, D. Bormann, A. Lucas, B. Denkena, C. Hackenbroich, A. Meyer-Lindenberg, Influence of different surface machining treatments of magnesium-based resorbable implants on the degradation behavior in rabbits, Adv. Eng. Mater. 11 (2009) B47-54.
[17] B. Denkena, A. Lucas, Biocompatible magnesium alloys as absorbable implant materials – adjusted surface and subsurface properties by machining processes, Ann. of the CIRP 56 (2007) 113-116.
[18] D.J. Bammann, M.L. Chicsa, G.C. Johnson, Modeling large deformation and failure in manufacturing processes, Theor. App. Mech. (1996) 359 – 376.
[19] D.J. Bammann, M.L. Chiesa, M.F. Horstemeyer, L.I. Weingarten, Failure in ductile materials using finite element methods, In: N. Jones, T. Wierzbicki (Eds.), Structural crashworthiness and failure, Elsevier, Essex, England (1993) 1-54.
[20] M. Salahshoor, Y.B. Guo, Cutting mechanics in high speed dry machining of biomedical magnesium-calcium alloy using internal state variable plasticity model, Int. J. Mach. Tool. Manuf. 51 (2011) 579-590.
[21] Y.B. Guo, Q. Wen, A hybrid modeling approach to investigate chip morphology transition with the stagnation effect by cutting edge geometry, Transactions of NAMRI/SME 33 (2005) 469-476.
[22] W.B. Palmer, R.C.K. Yeo, Metal flow near the tool point during orthogonal cutting with a blunt tool, Proc. 4th Int. Machine Tool Design & Res. Conf. (1963) 61-71.
[23] F.Z. Fang, H. Wu, W. Zhou, X.T. Hu, A study on mechanism of nano-cutting single crystal silicon, J. Mater. Proc. Tech. 184 (2007) 407-410.
[24] W. Grzesik, P. Nieslony, A computational approach to evaluate temperature and heat partition in machining with multilayer coated tools, Int. J. Mach. Tool. Manuf. 43 (2003) 1311-1317.
[25] H.E. Spear, J.P. Dismukes, Synthetic diamond – emerging CVD science and technology, Wiley, NY (1994).